# Anisotropic 2D Materials for Tunable Hyperbolic Plasmonics

Andrei Nemilentsau,[1] Tony Low,[2,*] and George Hanson[1]
[1]Department of Electrical Engineering & Computer Science, University of Wisconsin-Milwaukee, Milwaukee, Wisconsin 53211, USA
[2]Department of Electrical & Computer Engineering, University of Minnesota, Minneapolis, Minnesota 55455, USA
(Received 21 September 2015; published 10 February 2016)

Motivated by the recent emergence of a new class of anisotropic 2D materials, we examine their electromagnetic modes and demonstrate that a broad class of the materials can host highly directional hyperbolic plasmons. Their propagation direction can be manipulated on the spot by gate doping, enabling hyperbolic beam reflection, refraction, and bending. The realization of these natural 2D hyperbolic media opens up a new avenue in dynamic control of hyperbolic plasmons not possible in the 3D version.

DOI: 10.1103/PhysRevLett.116.066804

A hyperbolic material (HM) is a highly anisotropic material, with real parts of the principal components of its permittivity tensor having opposite signs [1,2]. The name of the material is derived from the topology of the $k$ surface, which is a hyperboloid (unlike an ellipsoid in conventional anisotropic materials [3]). Because of this unique topology, waves with very large (theoretically infinite) wave vectors can propagate inside HMs. The existence of the high-$k$ modes means a very large photonic density of states inside the material and thus these materials provide unique capabilities for controlling the properties of light emitters [4], creating broadband thermal sources [5], supporting directional surface plasmons [6,7], etc. All HMs known so far, both natural [8–12] and artificial [1,2], are nontunable materials with an optical response predefined by the design. The hyperbolic regime in metamaterials and metasurfaces relies entirely on the geometrical arrangement of the material constituents, and thus is extrinsic in nature. As the geometry of a metamaterial is difficult to modify after the material is created, its optical response at a given frequency cannot be changed on the spot.

In this Letter we argue that the emerging class of anisotropic 2D materials [13] is naturally suited to serve as HMs capable of supporting tunable hyperbolic plasmons. The family of 2D materials is very broad (encompassing many elements from the periodic table), with tremendous variety in electronic and optical properties, including metals, semimetals, semiconductors, and dielectrics [14]. Recently, an emerging class of 2D materials with anisotropic electronic and optical properties, such as group V mono- and multilayers, most notably black phosphorus (BP) [15–22], the 1T phase of the transition metal dichalcogenides [23–25], and the trichalcogenides [26–28], is garnering attention. Even though these materials are semiconductors with a band gap varying from the mid-IR to the optical range, injection of free carriers is possible by doping. Doping can be controlled by a gate, allowing for maximum carrier concentrations up to $10^{14}$ cm$^{-2}$ [29].

We offer a novel physical mechanism, inherent in nature, for creating highly tunable two-dimensional hyperbolic materials based on the anisotropic 2D materials in the far- and midinfrared frequency range. This mechanism relies on the interplay between two types of electron motions defining the electromagnetic response of typical semiconductors: the motion of electrons (holes) inside the conduction (valence) band of the material (intraband motion), and electron transitions from the valence to the conduction band of the material (interband transitions). In an isotropic material the predominance of intraband motions (interband transitions) renders a capacitive (inductive) response. We argue that, in novel highly anisotropic 2D materials, anisotropic electron motion results in an inductive material response along one of the optical axes, and a capacitive response along the other axis, thus effectively rendering a hyperbolic 2D material. As the intraband motion of electrons in 2D materials can be tuned on the spot by applying an electric bias, so can the optical response of the resulting 2D hyperbolic material. Moreover, due to its inherent nature, the hyperbolic regime can be implemented using a single sheet of the 2D material without requiring a complicated pattering of the substrate. We discuss the properties of these hyperbolic plasmons and examine their existence across the material parameter space.

We begin by considering a minimal model for the conductivity tensor for an anisotropic semiconducting medium, which accounts for both the intraband electron motions (first term on the right-hand side) and for the interband electron transitions (second term)

$$\underline{\underline{\sigma}} = \begin{pmatrix} \sigma_{xx} & 0 \\ 0 & \sigma_{yy} \end{pmatrix}, \tag{1}$$

where

$$\sigma_{jj} = \frac{ie^2}{\omega + i\eta}\frac{n}{m_j} + s_j\left[\Theta(\omega-\omega_j) + \frac{i}{\pi}\ln\left|\frac{\omega-\omega_j}{\omega+\omega_j}\right|\right], \tag{2}$$

$j = x, y$, where $n$ is the concentration of electrons, $m_j$ is the electron's effective mass along the $j$ direction, $\eta$ is a

 

relaxation time, $\omega_j$ is the frequency of the onset of interband transitions for the $j$ component of the conductivity, and $s_j$ accounts for the strength of the interband component. It may seem somewhat counterintuitive that the $x$ and $y$ components of the conductivity tensor can have different frequencies of the interband transitions. However, this is the case in BP multilayers, where different crystallographic directions have different symmetries, and thus the dipole moment for electron interband transitions is zero along one of the directions [18].

We use the Drude model in order to calculate the intraband conductivity. The interband conductivity is introduced phenomenologically by defining the absorption through a step function $\Theta(\omega-\omega_j)$. The imaginary part of the interband conductivity then follows from the Kramers-Kronig relations. In the general case, the parameters in Eq. (2) should be either measured experimentally or estimated theoretically using, for example, the Kubo formula. Assuming that the material parameters are isotropic, Eq. (2) can describe the conductivity of graphene [30]. On the other hand, in the anisotropic case this expression can be used as an approximation for the conductivity of multilayer black phosphorus [19,20].

We start our consideration with a particular set of parameters (see Fig. 1) and then study how the material response changes when one or several parameters vary. The conductivity of a 2D material is presented in Fig. 1. In general, two distinct regimes in the electromagnetic response of the 2D material can be identified. If the frequency is sufficiently low [to the left of dash-dotted red or blue lines in Fig. 1(a)], then the conductivity is of a pure Drude type ($\mathrm{Im}\sigma > 0$) and we refer to the material as purely anisotropic (in order to distinguish it from the material operating in hyperbolic anisotropic regime). If the frequency is sufficiently high the contribution from interband electron transitions may become dominant, and the imaginary part of the conductivity becomes negative. Because of the crystal asymmetry, $\mathrm{Im}\sigma_{xx}$ and $\mathrm{Im}\sigma_{yy}$ can in principle change sign at different frequencies, and a frequency interval where $\mathrm{Im}\sigma_{xx}\mathrm{Im}\sigma_{yy} < 0$ exists, which indicates the hyperbolic regime (to the right of dash-dotted red or blue lines). Such a natural hyperbolicity in anisotropic 2D materials is unlike hyperbolic metamaterials that have been extensively studied so far [1,6]. Moreover, 2D materials offer a unique opportunity of switching between the two different plasmonic regimes on the spot by applying an electrical bias [compare the two doping cases in Fig. 1(b)].

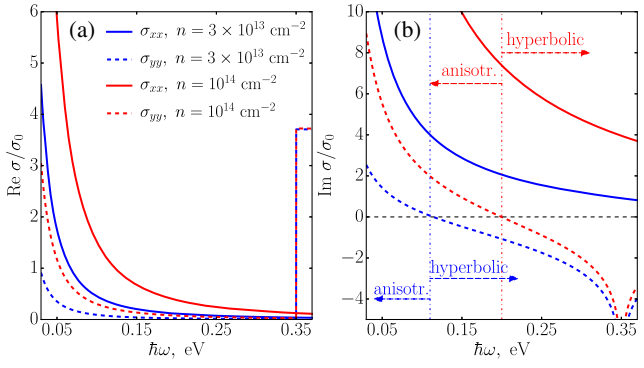


FIG. 1. Real (a) and imaginary (b) parts of the conductivity of the 2D material. The parameters of the 2D material are $m_x = 0.2m_0$, $m_y = m_0$, $\eta = 0.01$ eV, $w_x = 1$ eV, $s_x = 1.7s_0$, $w_y = 0.35$ eV, and $s_y = 3.7s_0$. $s_0 = e^2/4\hbar$; $m_0$ is the free-electron mass.

We study the properties of plasmons in pure anisotropic and hyperbolic regimes by exciting surface waves in a $2\times2$ $\mu$m sheet of a 2D material by a $y$-polarized electric dipole placed on top of the material (see Fig. 2 for details). We choose the material parameters to be the same as in Fig. 1. Hereinafter, we assume that the medium above and below the 2D material is vacuum. The distribution of the plasmon electric field (obtained by solving Maxwell's equations numerically using a commercial finite-difference time-domain method from Lumerical [31]) is presented in Figs. 2(a)–2(e). Figures 2(a) and 2(b) demonstrate the plasmon field intensity $\mathbf{E}$ in the purely anisotropic regime. In this case the plasmon propagates along one of the crystallographic axes of the material (the $x$ axis in this case). Figures 2(c)–2(e) show the plasmon propagation in

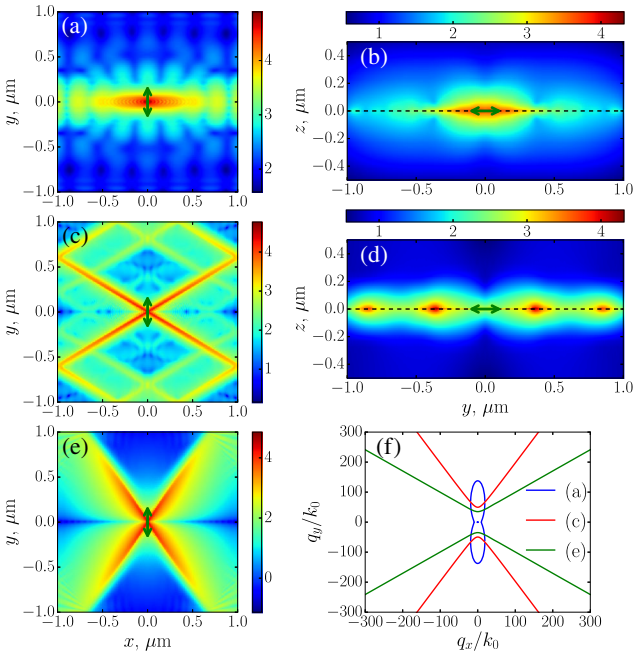


FIG. 2. (a)–(e) Spatial distribution (log scale) of the electric field $|\mathbf{E}|$ of a surface plasmon excited by a $y$-polarized electric dipole [green arrow in panels (a)–(e)] in a $2\times2$ $\mu$m sheet of a 2D material placed in the plane $z = 0$ [dashed black line in panels (b) and (d)]. The distribution of the electric field is calculated in the planes $z = 10$ nm (a),(c),(e) and $x = 0.6$ $\mu$m (b),(d). (a),(b) $n = 10^{14}$ cm$^{-2}$, $\hbar\omega = 0.165$ eV. (c),(d) $n = 10^{14}$ cm$^{-2}$, $\hbar\omega = 0.3$ eV. (e) $n = 3\times10^{13}$ cm$^{-2}$, $\hbar\omega = 0.3$ eV. (f) $k$ surfaces, $\omega(q_x, q_y) = \mathrm{const}$, for plasmons in panels (a)–(e).

the hyperbolic regime. The plasmon energy is channeled as very narrow beams, the angle between the direction of the beam propagation and the $x$ axis being a function of the electron concentration $n$. Thus, the direction of the plasmon propagation in the hyperbolic regime can be controlled on the spot by biasing the 2D material. This opens a new avenue for solving the problem of plasmon guiding, which in conventional materials requires structuring of the material geometry [32] or applying external magnetic fields [33,34].

In order to understand the behavior of surface waves it is instructive to inspect the plasmon dispersion relation in 2D materials. Considering only the eigenmodes bounded to the 2D material plane, $e^{i(q_x x+q_y y)}e^{\pm pz}$ (for $z\lesseqgtr 0$), we obtain [35]

$$(q_x^2-k_0^2)\sigma_{xx}+(q_y^2-k_0^2)\sigma_{yy}=2ip\omega\left(\varepsilon_0+\frac{\mu_0\sigma_{xx}\sigma_{yy}}{4}\right), \quad (3)$$

where $p=\sqrt{q_x^2+q_y^2-k_0^2}$, $k_0=\omega\sqrt{\varepsilon_0\mu_0}$ is the vacuum wave number, and $\varepsilon_0$, $\mu_0$ are the vacuum permittivity and permeability, respectively. The solution of Eq. (3), $\mathbf{q}(\omega)$, defines the plasmon wave front propagation. However, in anisotropic materials in the general case the directions of the wave front and energy propagation do not coincide. Instead, it is the group velocity $\mathbf{v}_g=\nabla_{\mathbf{q}}\omega(\mathbf{q})$ that is in the direction of the plasmon energy propagation [3]. The analytical computation of the group velocity requires the explicit form of $\omega(\mathbf{q})$, which is not available in our case. Instead, we use $k$ surfaces, $\omega(q_x,q_y)=\text{const}$, for further analysis [see Fig. 2(f)]. The group velocity, and thus the direction of the plasmon energy flow, has to be orthogonal to the $k$ surface. Assuming that the conductivity is purely imaginary $\sigma_{jj}=i\sigma''_{jj}$ (losses are small in our system, see Fig. 1) and that $q_x, q_y \gg k_0$, Eq. (3) can be further simplified:

$$\frac{q_x^2}{\sigma''_{yy}}+\frac{q_y^2}{\sigma''_{xx}}=2p\omega\left(\frac{\varepsilon_0}{\sigma''_{xx}\sigma''_{yy}}-\frac{\mu_0}{4}\right). \quad (4)$$

In the purely anisotropic case ($\sigma''_{xx}, \sigma''_{yy}>0$), if the right-hand side were constant, Eq. (4) would be an equation for an ellipse in $\mathbf{q}$ space with the axis oriented along $q_x$ and $q_y$. The length of the ellipse's principal axes along the $q_x$ ($q_y$) direction is proportional to $\sigma''_{yy}$ ($\sigma''_{xx}$). Thus, the $k$ surface always takes a quasielliptic form elongated along the direction of the smallest component of the conductivity tensor, the degree of elongation being defined by the ratio of $\sigma''_{xx}$ and $\sigma''_{yy}$. This is what we see in Fig. 2(f) (blue line), where $\sigma''_{xx}=0.55$ mS, $\sigma''_{yy}=0.039$ mS. Because of the strong elongation of the $k$ surface along the $q_y$ axis, the group velocity for the predominant range of the plasmon momentum $\mathbf{q}$ points approximately along the $q_x$ axis, which causes plasmons to carry energy in the direction of the $x$ crystallographic axis. If the ratio of $\sigma''_{xx}$ and $\sigma''_{yy}$ decreases, the plasmon beam spreads. Finally, in the case of $\sigma''_{xx}=\sigma''_{yy}$ the $k$ surface turns into a circle and there is no preferential direction for energy transfer.

In the hyperbolic case ($\sigma''_{xx}\sigma''_{yy}<0$) the $k$ surface is a hyperbola (see Fig. 2, red and green lines) with the hyperbola asymptotes being defined by $q_y=\pm q_x\sqrt{|\sigma''_{xx}/\sigma''_{yy}|}$ [see Eq. (4)]. Normals to the asymptotes always point along the same direction defined by

$$y=\pm x\sqrt{|\sigma''_{yy}/\sigma''_{xx}|}, \quad (5)$$

which is also the direction of the plasmon beams. As plasmons with all momenta carry energy along the same direction, the beams are significantly more localized than in the purely anisotropic case. Moreover, as can be seen from Eq. (5), the beams are leaning towards the crystallographic axis with the largest conductivity. From Fig. 1 it is clear that the conductivity of the 2D material, and thus the direction of the plasmon beam propagation, can be changed on the spot by doping. Indeed, in the case of Fig. 2(c) ($n=10^{14}$ cm$^{-2}$) $\sigma''_{xx}=0.3$ mS, $\sigma''_{yy}=-0.11$ mS, which corresponds to the propagation angle of 31°, while in the case presented in Fig. 2(e) ($n=3\times10^{13}$ cm$^{-2}$) $\sigma''_{xx}=0.076$ mS, $\sigma''_{yy}=-0.15$ mS, and the propagation angle is 55°. It should be noted that the propagation angles obtained using Eq. (5) agree with the results of numerical simulations presented in Fig. 2. Finally, we want to point out that the beam can experience multiple reflections from the edges of a 2D material sheet, as can be clearly seen from Fig. 2(c). This leads us to the discussion of the ray optics of the hyperbolic surface plasmons, reminiscent of conventional geometrical optics, in the later part of the Letter.

It should be noted that there is nothing special about the choice of the parameters in Figs. 1 and 2. Anisotropic and hyperbolic plasmons are supported by 2D materials with a broad range of parameters. It is quite obvious that as long as the material is anisotropic and has free electrons, pure anisotropic plasmons can propagate in this material when the frequency is sufficiently low. In fact, multilayer BP is an example of such a 2D material that is capable of guiding anisotropic plasmons [19].

The occurrence of a hyperbolic regime requires an interplay between electron intraband motion and interband transitions, as it is the interband transitions that cause the imaginary part of the conductivity to change sign. Thus, the hyperbolic regime comes into play at frequencies sufficiently close to the frequency of the interband transitions. In Fig. 3 we clarify this notion of closeness by considering the properties of hyperbolic plasmons for a broad range of parameters. We assume that $m_x<m_y$, which means that the $x$ component of the conductivity is predominantly Drude-like, while the $y$ component of the conductivity is the one that is mostly affected by the interband motions of electrons.

In Figs. 3(a) and 3(b) we inspect the behavior of surface plasmons at different frequencies and electron concentrations. One can see that the direction of the plasmon beams leans towards the $x$ axis at small frequencies and/or high concentrations. This is due to large values of $\sigma''_{xx}$, which is predominantly Drude-like [see Eq. (5)], compared to $\sigma''_{yy}$.

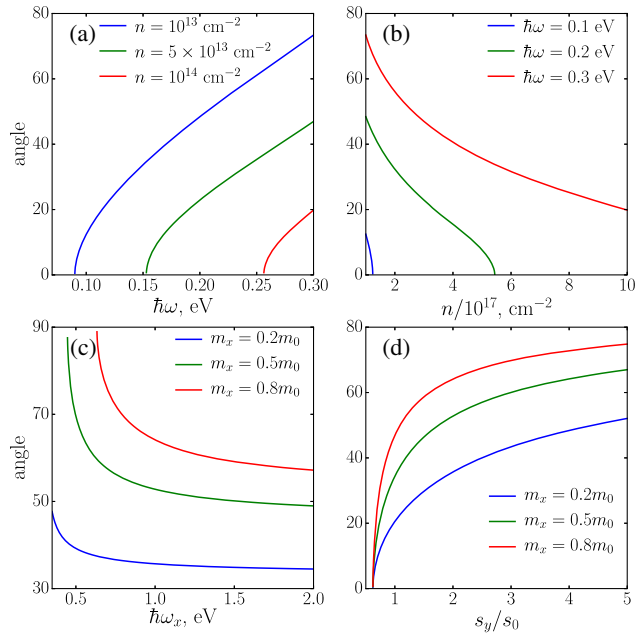


FIG. 3. Angle between plasmon beam direction and the $x$ axis, for $\eta = 0.01$ eV, $m_x = 0.2m_0$, $m_y = m_0$, $s_x = s_y = 2s_0$, $\hbar\omega_x = 1$ eV, $\hbar\omega_y = 0.35$ eV, $n = 5 \times 10^{13}$ cm$^{-2}$, and $\hbar\omega = 0.3$ eV, unless stated otherwise in the figure.

Moreover, when the frequency is very low and the electron concentration is very high, the intraband motion of electrons dominates $\sigma''_{yy}$ as well. This makes the material purely anisotropic [thus the cutoff in Figs. 3(a) and 3(b)]. On the other hand, at low concentrations and high frequencies, the interband motion of electrons is dominant. The conductivity $|\sigma''_{yy}|$ exceeds $|\sigma''_{xx}|$ and the plasmon beams propagate along directions close to the $y$ axis.

Figures 3(c) and 3(d) demonstrate the behavior of the plasmon beams at a given frequency and electron concentration, for different values of $m_x$, $\omega_x$, and $s_y$. One can see that any change in the set of parameters (decrease of $m_x$, increase of $\omega_x$) that leads to the dominance of the intraband motions of electrons over the interband ones shifts the directions of the plasmon beams towards the $x$ axis. When $\omega_x$ becomes high, the contribution of interband motions to $\sigma''_{xx}$ is negligible, and a further increase of $\omega_x$ does not change the propagation angle, thus the saturation shown in Fig. 3(c). On the other hand, the contribution of interband transitions to the conductivity increases with an increase in $s_y$, which explains the shift of the plasmon beam propagation direction towards the $y$ axis. In general, we can see that the hyperbolic regime in 2D materials is robust under a very broad range of experimentally achievable parameters.

Because of their outstanding mechanical properties, 2D materials can withstand a significant amount of strain, which provides unique capabilities to vary the material parameters in Eq. (2) over a wide range using strain engineering [36]. Indeed, significant variations in the band gap (between 0.38 and 2.07 eV) and electron effective mass (up to $4m_0$, and the relative magnitudes of $m_x$ and $m_y$ can be interchanged) in BP under the influence of strain [37–39] and/or an out-of-plane static electric field [21] were theoretically predicted and experimentally demonstrated [40]. The modification of the electronic and optical properties of $ReSe_2$ [24] and $TiS_3$ [28] under the influence of mechanical deformation was also reported. Another potential way of engineering material parameters consists in alloying 2D materials or creating heterostructures by stacking 2D materials vertically [41,42].

The realization of these natural 2D hyperbolic materials can potentially open up a new avenue in the dynamic control of hyperbolic surface waves not possible in the 3D version. In particular, in Fig. 4 we consider the propagation of plasmon rays through the interface between two sheets of a 2D material with different electron concentrations placed next to each other. We can clearly see the reflection and refraction of the plasmons at the interface, with the reflection angle being equal to the incident angle and the refraction angle being defined by the conductivity of the second medium. Moreover, for a plasmon beam incident from the region of higher electron concentration [Fig. 4(a)] most of the plasmon's energy is transferred through the interface to the lower doped medium. In the opposite case [Fig. 4(b)], most of the plasmon's energy is reflected back to the lower doped medium. Finally, we implement an analogue of a graded-index plasmonic material by gradually varying the doping across $y$ from $10^{14}$ to $2 \times 10^{13}$ cm$^{-2}$ [see Fig. 4(c)]. One can see the

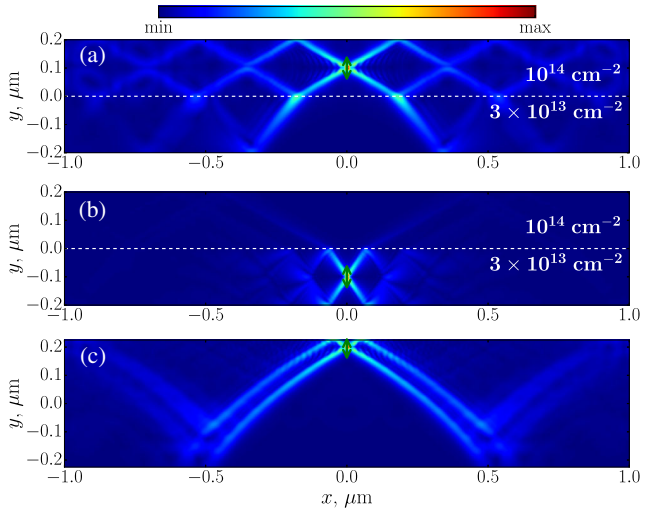


FIG. 4. Plasmon launched by a $y$-polarized electric dipole in a layered medium made by placing sheets of 2D materials with different electron concentrations next to each other. The dipole position is designated by a green arrow. The parameters of the 2D materials are the same as in Fig. 1. (a),(b) The concentration of electrons in the material above the dashed white line is $n = 10^{14}$ cm$^{-2}$, while below the white line it is $n = 3 \times 10^{13}$ cm$^{-2}$. (c) The electron concentration varies gradually from $n = 10^{14}$ cm$^{-2}$ (upper layer) to $n = 2 \times 10^{13}$ cm$^{-2}$ (lower layer).

bending of the plasmon ray resembling the bending of the light ray in a graded-index medium.

In conclusion, we demonstrated in a general manner for the first time that anisotropic 2D materials can support the propagation of highly directional and tunable hyperbolic surface waves. In the purely anisotropic regime ($\mathrm{Im}\sigma''_{xx} > 0$, $\mathrm{Im}\sigma''_{yy} > 0$) the plasmons propagate along the crystallographic axis with a larger conductivity, with the ratio of the imaginary parts of the conductivities defining the degree of plasmon localization along the axis. In the hyperbolic regime ($\mathrm{Im}\sigma''_{xx}\mathrm{Im}\sigma''_{yy} < 0$), the plasmons propagate as a very localized beam along the direction defined by the ratio of the imaginary parts of the conductivities. Unlike 3D HMs, the new 2D natural HMs are highly tunable; the frequency range of the hyperbolic regime as well as the direction of the plasmon beam propagation can be modified on the spot by gate doping of the 2D material. Through doping control, reflection, refraction, and bending of the plasmon beams can be achieved. By elucidating the existence of an interesting hyperbolic regime due to the interplay of intra- and interband electron motion, we hope this will inspire and guide an experimental search and verification.

*tlow@umn.edu


[1] A. Poddubny, I. Iorsh, P. Belov, and Y. Kivshar, Nat. Photonics **7**, 948 (2013).
[2] L. Ferrari, C. Wu, D. Lepage, X. Zhang, and Z. Liu, Prog. Quantum Electron. **40**, 1 (2015).
[3] J. Kong, *Electromagnetic Wave Theory* (Wiley-Interscience, New York, 1986).
[4] C. L. Cortes, W. Newman, S. Molesky, and Z. Jacob, J. Opt. **14**, 063001 (2012).
[5] Y. Guo and Z. Jacob, Opt. Express **21**, 15014 (2013).
[6] J. S. Gomez-Diaz, M. Tymchenko, and A. Alù, Phys. Rev. Lett. **114**, 233901 (2015).
[7] O. Y. Yermakov, A. I. Ovcharenko, M. Song, A. A. Bogdanov, I. V. Iorsh, and Y. S. Kivshar, Phys. Rev. B **91**, 235423 (2015).
[8] S. Dai, Z. Fei, Q. Ma, A. S. Rodin, M. Wagner, A. S. McLeod, M. K. Liu, W. Gannett, W. Regan, K. Watanabe, T. Taniguchi, M. Thiemens, G. Dominguez, A. H. C. Neto, A. Zettl, F. Keilmann, P. Jarillo-Herrero, M. M. Fogler, and D. N. Basov, Science **343**, 1125 (2014).
[9] J. D. Caldwell, A. V. Kretinin, Y. Chen, V. Giannini, M. M. Fogler, Y. Francescato, C. T. Ellis, J. G. Tischler, C. R. Woods, A. J. Giles, M. Hong, K. Watanabe, T. Taniguchi, S. A. Maier, and K. S. Novoselov, Nat. Commun. **5**, 5221 (2014).
[10] J. Sun, N. M. Litchinitser, and J. Zhou, ACS Photonics **1**, 293 (2014).
[11] P. Li, M. Lewin, A. V. Kretinin, J. D. Caldwell, K. S. Novoselov, T. Taniguchi, K. Watanabe, F. Gaussmann, and T. Taubner, Nat. Commun. **6**, 7507 (2015).
[12] A. Kumar, T. Low, K. H. Fung, P. Avouris, and N. X. Fang, Nano Lett. **15**, 3172 (2015).
[13] H. Zhang, ACS Nano **9**, 9451 (2015).
[14] P. Miro, M. Audiffred, and T. Heine, Chem. Soc. Rev. **43**, 6537 (2014).
[15] H. Liu, A. T. Neal, Z. Zhu, Z. Luo, X. Xu, D. Tomnek, and P. D. Ye, ACS Nano **8**, 4033 (2014).
[16] L. Li, Y. Yu, G. J. Ye, Q. Ge, X. Ou, H. Wu, D. Feng, X. H. Chen, and Y. Zhang, Nat. Nanotechnol. **9**, 372 (2014).
[17] A. S. Rodin, A. Carvalho, and A. H. Castro Neto, Phys. Rev. Lett. **112**, 176801 (2014).
[18] J. Qiao, X. Kong, Z.-X. Hu, F. Yang, and W. Ji, Nat. Commun. **5**, 4475 (2014).
[19] T. Low, R. Roldán, H. Wang, F. Xia, P. Avouris, L. M. Moreno, and F. Guinea, Phys. Rev. Lett. **113**, 106802 (2014).
[20] T. Low, A. S. Rodin, A. Carvalho, Y. Jiang, H. Wang, F. Xia, and A. H. Castro Neto, Phys. Rev. B **90**, 075434 (2014).
[21] Y. Li, S. Yang, and J. Li, J. Phys. Chem. C **118**, 23970 (2014).
[22] B. Liu, M. Kpf, A. N. Abbas, X. Wang, Q. Guo, Y. Jia, F. Xia, R. Weihrich, F. Bachhuber, F. Pielnhofer, H. Wang, R. Dhall, S. B. Cronin, M. Ge, X. Fang, T. Nilges, and C. Zhou, Adv. Mater. **27**, 4423 (2015).
[23] S. Tongay, H. Sahin, C. Ko, A. Luce, W. Fan, K. Liu, J. Zhou, Y.-S. Huang, C.-H. Ho, J. Yan, D. F. Ogletree, S. Aloni, J. Ji, S. Li, J. Li, F. M. Peeters, and J. Wu, Nat. Commun. **5**, 3252 (2014).
[24] S. Yang, C. Wang, H. Sahin, H. Chen, Y. Li, S.-S. Li, A. Suslu, F. M. Peeters, Q. Liu, J. Li, and S. Tongay, Nano Lett. **15**, 1660 (2015).
[25] D. A. Chenet, O. B. Aslan, P. Y. Huang, C. Fan, A. M. van der Zande, T. F. Heinz, and J. C. Hone, Nano Lett. **15**, 5667 (2015).
[26] J. O. Island, M. Buscema, M. Barawi, J. M. Clamagirand, J. R. Ares, C. Snchez, I. J. Ferrer, G. A. Steele, H. S. J. van der Zant, and A. Castellanos-Gomez, Adv. Opt. Mater. **2**, 641 (2014).
[27] J. Dai and X. C. Zeng, Angew. Chem. **127**, 7682 (2015).
[28] J. Kang, H. Sahin, H. D. Ozaydin, R. T. Senger, and F. M. Peeters, Phys. Rev. B **92**, 075413 (2015).
[29] D. K. Efetov and P. Kim, Phys. Rev. Lett. **105**, 256805 (2010).
[30] F. H. L. Koppens, D. E. Chang, and F. J. G. de Abajo, Nano Lett. **11**, 3370 (2011).
[31] Lumerical Solutions, Inc, http://www.lumerical.com/tcad-products/fdtd/.
[32] E. Moreno, S. G. Rodrigo, S. I. Bozhevolnyi, L. Martín-Moreno, and F. J. García-Vidal, Phys. Rev. Lett. **100**, 023901 (2008).
[33] Y. Hadad and B. Z. Steinberg, Phys. Rev. Lett. **105**, 233904 (2010).
[34] Y. Mazor and B. Z. Steinberg, Phys. Rev. B **86**, 045120 (2012).
[35] G. Hanson, IEEE Trans. Antennas Propag. **56**, 747 (2008).
[36] R. Roldan, A. Castellanos-Gomez, E. Cappelluti, and F. Guinea, J. Phys. Condens. Matter **27**, 313201 (2015).
[37] X. Han, H. M. Stewart, S. A. Shevlin, C. R. A. Catlow, and Z. X. Guo, Nano Lett. **14**, 4607 (2014).
[38] R. Fei and L. Yang, Nano Lett. **14**, 2884 (2014).
[39] D. Çakır, H. Sahin, and F. M. Peeters, Phys. Rev. B **90**, 205421 (2014).
[40] J. Kim, S. S. Baik, S. H. Ryu, Y. Sohn, S. Park, B.-G. Park, J. Denlinger, Y. Yi, H. J. Choi, and K. S. Kim, Science **349**, 723 (2015).
[41] A. K. Geim and I. V. Grigorieva, Nature (London) **499**, 419 (2013).
[42] Q. Zeng, H. Wang, W. Fu, Y. Gong, W. Zhou, P. M. Ajayan, J. Lou, and Z. Liu, Small **11**, 1868 (2015).